

Journal of Materials Chemistry A

Accepted Manuscript



This is an *Accepted Manuscript*, which has been through the Royal Society of Chemistry peer review process and has been accepted for publication.

Accepted Manuscripts are published online shortly after acceptance, before technical editing, formatting and proof reading. Using this free service, authors can make their results available to the community, in citable form, before we publish the edited article. We will replace this *Accepted Manuscript* with the edited and formatted *Advance Article* as soon as it is available.

You can find more information about *Accepted Manuscripts* in the [Information for Authors](#).

Please note that technical editing may introduce minor changes to the text and/or graphics, which may alter content. The journal's standard [Terms & Conditions](#) and the [Ethical guidelines](#) still apply. In no event shall the Royal Society of Chemistry be held responsible for any errors or omissions in this *Accepted Manuscript* or any consequences arising from the use of any information it contains.

Cite this: DOI: 10.1039/c0xx00000x

www.rsc.org/xxxxxx

ARTICLE TYPE

Polystyrene foam to high-performance doped carbon catalyst with ultrahigh surface area and hierarchical porous structures for oxygen reduction†

Chenghang You^a, Shijun Liao^{a*}, Xiaochang Qiao^a, Xiaoyuan Zeng^a, Fangfang Liu^a, Ruiping Zheng^a,
Huiyu Song^a, Jianhuang Zeng^a, Yingwei Li^a

Received (in XXX, XXX) Xth XXXXXXXXX 20XX, Accepted Xth XXXXXXXXX 20XX

DOI:

A high-performance doped carbon catalyst with ultrahigh surface area (1123 m² g⁻¹) and hierarchical porous structures was prepared through an economical, non-template pyrolyzing approach using cross-linked polystyrene, melamine and iron chloride as precursors. The catalyst exhibits excellent oxygen reduction reaction (ORR) performance, outstanding methanol tolerance, remarkable stability, and high catalytic efficiency (nearly 100% selectivity for the four-electron ORR process). Remarkably, its ORR activity can even surpass that of commercial Pt/C catalyst in alkaline media, with a half-wave potential 20 mV more positive. To our knowledge, it is also one of the most active ORR catalysts in alkaline media to date. By investigating the effects of N dopants and Fe residue on the catalyst's ORR performance, we find that residual Fe is as important as doped nitrogen in enhancing ORR performance. The catalyst's high ORR performance, outstanding stability and excellent methanol tolerance, combined with its hierarchical porous morphology, make it promising for the application in novel, environmentally friendly electrochemical energy systems. This research also provides a potential way to turn waste into wealth.

Introduction

Oxygen reduction reaction (ORR) plays a critical role in novel, high-efficiency and environmentally friendly electrochemical energy systems, such as proton exchange membrane fuel cells (PEMFCs), direct methanol fuel cells (DMFC), metal-air batteries, etc. To date, Pt is still the most efficient and widely used catalyst for ORR. However, its high cost, low methanol tolerance and limited stability still blocks the commercialization of these novel energy systems. Thus, it is extremely important to develop efficient non-precious catalysts to substitute Pt. For this purpose, many materials have been proposed¹⁻⁹. Among these materials, doped carbons attract significant attention due to their high activity and low cost^{4-8, 10-14}. Although great progress has been made in this field during the past several years, there is still a long way to go before these catalysts are feasible in practical applications.

Highly porous carbon materials have been widely used in gas adsorption, separation, catalysis, and organic conversion^{4, 15-18}. Especially, mesoporous carbon materials are popular in the fields of electrochemical energy storage and conversion due to their unique structural features, which can offer high surface areas for large numbers of potential active sites, as well as numerous channels for mass transfer¹⁹⁻²¹. It has also been confirmed that

enlarged pores can facilitate the ORR²³. Qiao and co-workers found that ORR activity could be remarkably enhanced by simply enlarging the pores in a carbon-based material from meso-size (12 nm) to macro-size (150 nm)²².

There is no doubt that macropores can improve mass transfer and enhance the ORR. However, it is also well known that macroporous structures usually result in relatively low surface areas, which will certainly limit the number of exposed potential active sites (another important factor for ORR enhancement)²³. To resolve the conflict between high accessibility and high surface area, hierarchical porous carbons (HPCs) with abundant micropores located in the walls of mesopores and macropores are promising candidates, since they can simultaneously provide micropores for active site exposure, along with mesopores and macropores for efficient mass transfer.

Generally, HPCs are prepared by using templating methods, activating methods or methods combining the two techniques²⁴⁻³⁰. However, these approaches usually require special pore-forming processes, such as template removal (for hard-templating methods), special nanostructure fabrication (for soft-templating methods), and post-activation treatments (for methods containing activating procedures). These pore-forming processes typically make the preparation procedures tedious. Hence, non-template methods that require no further activating processes can be

attractive for the preparation of HPCs. To our knowledge, there are few published reports on carbon-based ORR catalysts with hierarchical porous structures prepared through non-template methods.

In this work, we constructed a material with a high surface area and hierarchical porous structures through a facile template-free approach by using polystyrene (PS) foam as the precursor, which is widely used in packaging and a major source of “white pollution”. The as-prepared material exhibited excellent ORR performance: compared to commercial Pt/C catalyst, its half-wave potential was 20 mV more positive and its current density was 1.24 mA cm⁻² higher at -0.2 V (vs. Ag/AgCl). Besides its excellent ORR performance, it also showed remarkable stability, outstanding methanol tolerance, and high catalytic efficiency (nearly 100% selectivity for the four-electron ORR process). By investigating the effects of N dopants and Fe residue on the catalyst’s ORR performance, we found that Fe residue plays an important role in the enhancement of ORR catalytic activity, which can be even comparable to that of active nitrogen.

Experimental section

Preparation of materials

The typical preparation of the Fe-Mel-CPS catalyst was described as follows. First, the polystyrene (PS) precursor was cross-linked through a Friedel–Crafts (F–C) reaction using tetrachloride (CCl₄) as the cross-linker and aluminum chloride (AlCl₃) as the catalyst³¹. Briefly, 5.0 g PS foam was dissolved in 400 mL CCl₄, and then 12.0 g AlCl₃ was added. The mixture was then refluxed under magnetic stirring for 48 h to undergo an F–C reaction, followed by filtrating, rinsing with hydrochloric acid alcohol solution and deionized (DI) water, and, finally drying at 110°C. We refer to the obtained cross-linked PS as CPS.

The doped carbon catalysts were prepared through the two-stage pyrolysis of a mixture of CPS, melamine, and ferric trichloride (FeCl₃). Briefly, a suspension containing 1.0 g CPS, 2.0 g melamine, 1.0 g FeCl₃, and 200 mL DI water was evaporated at 80°C under magnetic stirring. The obtained composite powder was first treated at 550 °C for 4 h using a heating rate of 2 °C min⁻¹ and then pyrolyzed at 900 °C for 1 h in Ar flow, followed by leaching in 0.5 M H₂SO₄ at 80 °C for 8 h, and annealing at 900 °C for another 2 h in Ar flow. The as-prepared catalyst is referred to Fe-Mel-CPS here.

For comparison, another two catalysts (one derived directly from CPS without any additives in the precursor, and the other derived from a mixture of CPS and melamine without any Fe being added) were prepared using the same procedures as for Fe-Mel-CPS. These finally obtained two catalysts are called C-CPS and Mel-CPS, respectively.

Characterization

Scanning electron microscopy (SEM) was conducted on a Nova Nano 430 field emission scanning electron microscope (FEI, Netherlands). Transmission electron microscopy (TEM) images were recorded on a JEM-2100 transmission electron microscope (JEOL, Japan). X-ray diffraction (XRD) was conducted on a TD-3500 powder diffractometer (Tongda, China). X-ray photoelectron spectroscopy (XPS) was performed on an ESCALAB 250 X-ray photoelectron spectrometer (Thermo-VG

Scientific, USA). Specific surface areas and pore-size distributions were measured by Brunauer-Emmett-Teller (BET) nitrogen adsorption-desorption at 77 K on a Tristar II 3020 gas adsorption analyzer (Micromeritics, USA). Analysis on carbonyl bridges was carried out on a Bruker Equinox 55 Fourier transform infrared (FTIR) spectrometer. The amounts of Fe present in the catalysts were determined using inductively coupled plasma-atomic emission spectrometry (ICP-AES) analysis with a Prodigy ICP-AES system (Leeman Labs Inc., USA).

Electrochemical testing

Electrochemical measurements were conducted in a standard three-electrode glass cell on an electrochemical workstation (Ivium, Netherlands) at room temperature, coupled with a rotating disk electrode (RDE) system (PINE Research Instruments, USA). A glassy carbon electrode (GCE, with a diameter of 5 mm and an electrode area of 0.1964 cm²) was used as the working electrode substrate, with Ag/AgCl/KCl (3 M) and Pt wire as the reference electrode and counter electrode, respectively. For simplicity, the Ag/AgCl/KCl (3 M) reference electrode is hereafter abbreviated to Ag/AgCl.

Before every measurement, the GCE surface was cleaned by ultrasonication in ethanol and polishing with α-Al₂O₃ slurry (50 nm) on a microcloth, followed by rinsing with DI water and drying under an infrared lamp.

A slurry of the active material was prepared by mixing 5.0 mg catalyst with 1 mL of an ethanol solution containing Nafion (0.25 wt%) under ultrasonication. Next, 20 μL catalyst slurry was pipetted onto the surface of the GCE, followed by drying under an infrared lamp to form a catalyst film on the GCE substrate. The catalyst loading was approximately 0.5 mg cm⁻².

Cyclic voltammetry (CV) and linear sweep voltammetry (LSV) measurements were conducted in 0.1 M KOH solution at a scan rate of 5 mV s⁻¹. The LSV curves were recorded at a disk rotation rate ranging from 1600 to 3600 rpm. Before every measurement, the KOH solution was saturated with pure N₂ (99.999%) or pure O₂ (99.999%) for at least 30 min. All the current densities were normalized to the geometric area of the GCE. The chronoamperometric response was obtained at -0.3 V (vs. Ag/AgCl) in an O₂-saturated 0.1 M KOH solution.

The electron transfer number per oxygen molecule involved was calculated based on the Koutecky–Levich (K–L) equation as follows:

$$J^{-1} = J_L^{-1} + J_K^{-1} = B^{-1}\omega^{-1/2} + J_K^{-1}$$

$$B = 0.62nFC_0D_0^{2/3}\nu^{-1/6}$$

$$J_K = nF\kappa C_0$$

where J is the measured current density; J_K and J_L are the kinetic and diffusion limiting current densities, respectively; ω is the angular velocity of the disk ($\omega = 2\pi N$, where N refers to the linear rotation rate); n is the electron transfer number involved in the reduction procedure of one O₂ molecule; F is the Faraday constant ($F = 96\,485\text{ C mol}^{-1}$); C_0 is the bulk concentration of O₂; D_0 is the diffusion coefficient of O₂ in the KOH electrolyte; ν is the kinetic viscosity of the electrode; and κ is the electron transfer rate constant; n and J_K were obtained from the slope and intercept of the K–L plots, respectively. By using the values $C_0 = 1.2 \times 10^{-3}\text{ mol L}^{-1}$, $D_0 = 1.9 \times 10^{-5}\text{ cm}^2\text{ s}^{-1}$, and $\nu = 0.01\text{ cm}^2\text{ s}^{-1}$ (in 0.1 M KOH solution), the electron transfer number (n) was calculated.

For the Tafel plots, the kinetic current was calculated from the mass-transport correction of the RDE using the following equation:

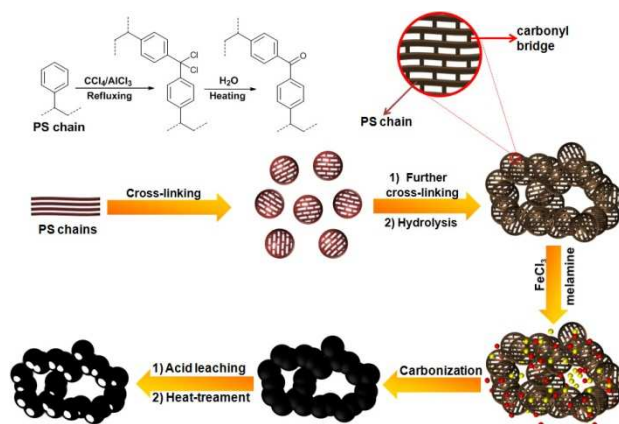
$$I_k = |I_L I(I_L - I)^{-1}|$$

5 Results and discussion

The procedure for preparing our PS foam-derived catalyst is illustrated in Scheme 1.

First, single PS chains are interlinked by $-CCl_2-$ bridges through the F-C reaction to form cross-linking polystyrene particles. These particles then interconnect in different directions to form a three-dimensional network, while the stacking of the particles creates porous structures.

During the drying procedure, the $-CCl_2-$ groups were spontaneously hydrolyzed into carbonyl bridges, which were confirmed by the absorption peaks of the carbonyl group around 1700 cm^{-1} in the FTIR spectra (Fig. 1). The cross-linking procedure is a very important step for the preparation of this high-performance catalyst, since the PS chains will decompose into styrene monomer below their annealing temperature if they are not cross-linked. The formation of stable carbonyl bridges is also believed to be important for maintaining the porous structures during the later heat-treatment procedure.



Scheme 1 Schematic diagram of the doped carbon catalyst preparation process

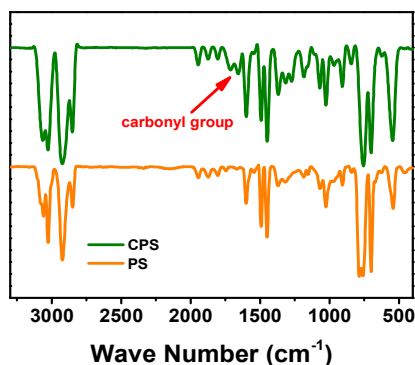


Fig. 1 FTIR spectra of PS and CPS

SEM image of the CPS (Fig. 2a) shows that the CPS nanoparticles are generated through the cross-linking reaction,

and the hierarchical porous structures are fabricated by the stacking of these nanoparticles. The SEM images of the three as-prepared materials all exhibit macro- or meso-pores (Fig. 2b, 2c, S1), indicating the existence of porous structures. From these images one can also observe differences in the materials' morphologies: the dispersion of the Mel-CPS (Fig. S1) is obviously better than that of CPS (Fig. 2b), which can be attributed to the addition of melamine; in the case of Fe-Mel-CPS, some sheet-like structures can be found (Fig. 2c), which are also visible in the TEM image (Fig. 2d).

Regarding the TEM images (Fig. 2d, S1), it is interesting that Fe-Mel-CPS has quite different structures compared with the other two materials (Fig. S1). It exhibits porous, bubble-like structures with very thin walls, which might be attributable to the addition of Fe^{3+} . It is expected that such structure will yield a higher surface area.

The existence of Fe residues in the catalyst can be detected by XRD, which exists as Fe, Fe_3C and Fe_3O_4 (see Fig. 3)³³. Furthermore, a few of Fe related nanoparticles can be observed by HRTEM. Fig. 2e shows such a particle with size of ca. 15nm. From its further magnified images (Fig. 2e and 2f), we can see that the spacing of the lattice fringes of the particle is about 0.204 nm, which can be assigned to Fe or Fe_3C species within measurement error³³, which is consistent with the XRD results³³.

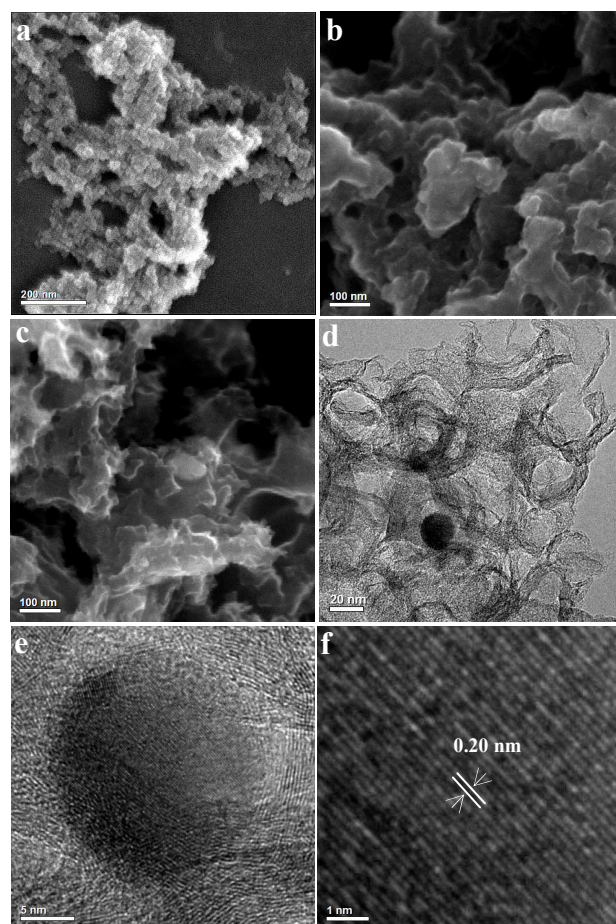


Fig. 2 SEM images: (a) CPS; (b) C-CPS; (c) Fe-Mel-CPS; (d) TEM image of Fe-Mel-CPS; (e, f) HRTEM of Fe-Mel-CPS.

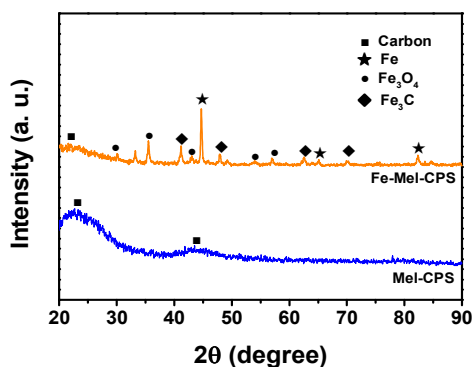


Fig. 3 XRD patterns of different Fe-Mel-CPS and Mel-CPS

Fig. 4a shows the N_2 gas adsorption-desorption isotherms of Fe-Mel-CPS. It can be observed that the isotherm of Fe-Mel-CPS exhibits a type IV curve, with a hysteresis loop in the medium- and high-pressure region, indicating that the material contains both micropores and mesopores. The pore-size distribution of Fe-Mel-CPS obtained from the N_2 adsorption-desorption isotherms (Fig. 4b) shows a higher pore density in the mesopore region, confirming that it contains abundant mesoporous structures.

It should be pointed out that the isotherms and pore-size distributions of the other samples (CPS, C-CPS, Mel-CPS) also suggest that there are both micro- and mesoporous structures in those three materials (Fig. S2), indicating that the macroscopically porous structures can be easily inherited from the CPS.

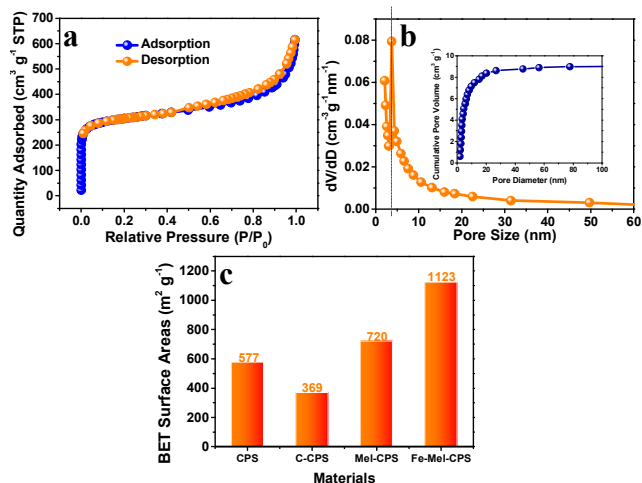


Fig. 4 (a) N_2 adsorption-desorption isotherms of Fe-Mel-CPS; (b) pore-size distributions and cumulative pore volume (inserted figures) of Fe-Mel-CPS, calculated using the Barrett-Joyner-Halenda (BJH) method; (c) BET surface areas of the various materials

Regarding the surface areas of the four materials (Fig. 4c), Fe-Mel-CPS has the largest surface area of $1123 \text{ m}^2 \text{ g}^{-1}$; C-CPS has the lowest at $369 \text{ m}^2 \text{ g}^{-1}$, even lower than that of CPS ($577 \text{ m}^2 \text{ g}^{-1}$). This decrease in surface area, we suggest, should be attributed to the aggregation of microparticles and the collapse of partial microstructures during the pyrolysis procedure. Mel-CPS has almost twice the surface area of C-CPS. Obviously, adding melamine to the precursor can increase the surface area of the

final product. The highest surface area of Fe-Mel-CPS ($1123 \text{ m}^2 \text{ g}^{-1}$) suggests that the addition of Fe to the precursor can further increase carbon's surface area.

Fig. 5a shows the XPS survey spectra of the Mel-CPS and Fe-Mel-CPS catalysts. The catalyst composition data, based on the XPS spectra, are summarized in Table 1, where we can see that Mel-CPS has a much higher N content (2.57 at%) than Fe-Mel-CPS does (1.70 at%).

Fig. 5b and 5c show the high-resolution XPS spectra of Mel-CPS and Fe-Mel-CPS, and the deconvolution results of each spectrum. Table 2 presents the contents of each N type in the two obtained catalysts by integrating each of the deconvolution peaks for each sample.

It is clear that the addition of Fe can significantly enhance the amounts of pyridinic and pyrrolic N. The relative content of pyridinic N increases from 38.2 at% in Mel-CPS to 60.6 at% in Fe-Mel-CPS. Plus, adding Fe seems to restrain the formation of inactive oxidized N; the relative content of oxidized N in Fe-Mel-CPS is only 8.2 at%, compared with 27.8 at% in Mel-CPS.

By multiplying the net N content of each catalyst by the relative amounts of each N species, we obtained the content of each N species for each sample. As shown in Fig. 5d, the two catalysts have almost the same amounts of pyrrolic and pyridinic N, although their oxidized, graphitic, and total N amounts are different. As we will discuss later, the Fe-Mel-CPS catalyst exhibits much higher ORR performance than Mel-CPS. It remains to ask what causes such a difference in ORR performance, and we will discuss this in the following section.

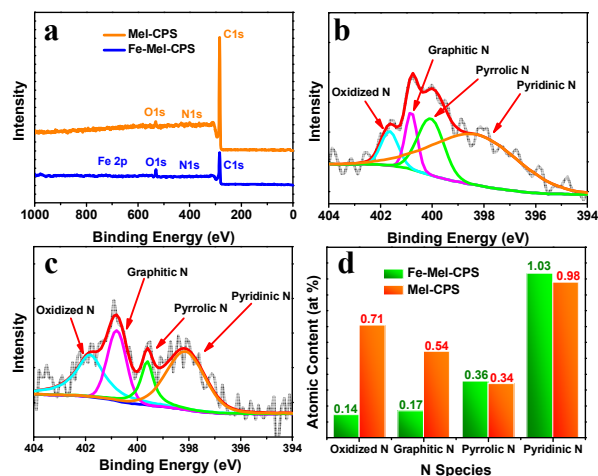


Fig. 5 (a) XPS survey spectra of Mel-CPS and Fe-Mel-CPS catalysts; (b) high-resolution N1s XPS spectrum of Fe-Mel-CPS and its deconvolution spectra; (c) high-resolution N1s XPS spectrum of Mel-CPS and its deconvolution spectra; (d) atomic content of each N species in Mel-CPS and Fe-Mel-CPS

Table 1 Surface composition of Mel-CPS and Fe-Mel-CPS, calculated from XPS results^a

	Species concentration (at%)			
	C	O	N	Fe
Fe-Mel-CPS	88.3	8.76	1.70	0.98
Mel-CPS	95.85	1.43	2.57	—

^aHydrogen is not taken into account for the calculations.

Table 2 Distribution of each N species, obtained from the fitting results of N1s XPS spectra (normalized to the surface N atoms of each material)

	Species concentration (at%)			
	Oxidized N	Graphitic N	Pyrolic N	Pyridinic N
Fe-Mel-CPS	8.2	10.0	21.2	60.6
Mel-CPS	27.6	21.0	13.2	38.2

Fig. 6a shows the CV curves of the three catalysts in N_2 -saturated and O_2 -saturated 0.1 M KOH solution. Fe-Mel-CPS demonstrates the best ORR performance, with a peak potential of -0.13 V and a peak current density of 1.13 mA cm^{-2} . In fact, the doped carbon derived from CPS exhibits certain ORR activity. The addition of melamine improves the performance of the catalyst significantly (with a peak potential 30 mV more positive than that of C-CPS), and the further addition of Fe enhances the ORR performance even more (yielding a peak potential 90 mV more positive than that of Mel-CPS). It is important to note that the improvement resulting from the addition of Fe is much stronger than sole melamine.

Fig. 6b and 6c illustrate the LSV curves of the three catalysts in O_2 -saturated 0.1 M KOH solution at an electrode rotation rate of 1600 rpm. For comparison, the ORR performance of commercial Pt/C catalyst (20 wt% Pt, Johnson Matthey, UK) was also tested under the same conditions. It is exciting that the ORR activity of Fe-Mel-CPS catalyst was obviously superior, with a half-wave potential 20 mV more positive than that of commercial Pt/C. To our knowledge, it is also one of the best doped carbon ORR catalysts to date.

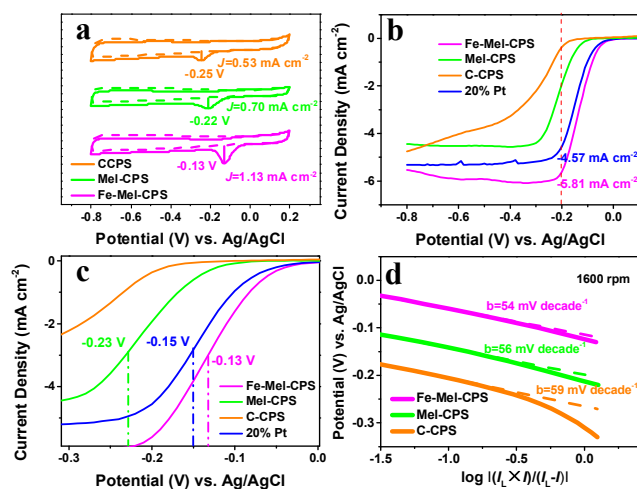
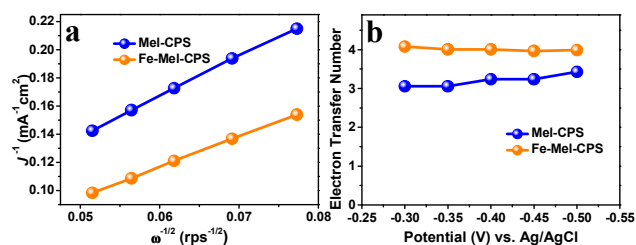
**Fig. 6** Electrochemical measurements of C-CPS, Mel-CPS, and Fe-Mel-CPS: (a) CVs; (b) LSVs; (c) magnification of the LSV curves; (d) Tafel plots of the three materials

Fig. 6d shows the Tafel plots of the three catalysts, derived from mass-transport correction of the corresponding RDE data. The Tafel slopes of Fe-Mel-CPS, Mel-CPS, and C-CPS are 54, 56 and 59 mV $decade^{-1}$, respectively. The lowest Tafel slope of Fe-Mel-CPS, confirms the superior ORR activity of that catalyst. To further understand the kinetics of the ORR on our catalysts, we recorded the LSV curves of Mel-CPS and Fe-Mel-CPS in O_2 -saturated 0.1 M KOH solution at different rotation rates (Fig. S3) and further analyzed the LSV data using the K-L equations.

The K-L plots of the two materials at a potential of -0.5 V (vs.

Ag/AgCl) are shown in Fig. 7a. Obviously, Fe-Mel-CPS has a lower slope, suggesting that it has a higher electron transfer number. By using the K-L equations, we calculated the exact electron transfer numbers (n) under varying potentials with Fe-Mel-CPS and Mel-CPS. And these values are summarized in Fig. 7b. The average electron transfer numbers are calculated to be 4.0 and 3.2 for Fe-Mel-CPS and Mel-CPS, respectively. That is, on the Fe-Mel-CPS catalyst, oxygen can be directly reduced to OH^- by accepting four electrons without producing the OOH^- intermediate (four-electron path), while Mel-CPS can only catalyze the ORR through a path combining two-electron and four-electron processes, implying that Fe-Mel-CPS is a much better ORR catalyst than Mel-CPS.

**Fig. 7** (a) K-L plots of Mel-CPS and Fe-Mel-CPS at -0.5 V (vs. Ag/AgCl); (b) electron transfer numbers of Mel-CPS and Fe-Mel-CPS

It is interesting that C-CPS, containing no N or Fe, also exhibits remarkable ORR activity, which might properly be attributed to the co-effects of special morphology and impurities³⁴ (such as Al, O and Cl dopants, induced during the preparation of CPS).

It is clear that N doping can drastically improve catalysts' ORR activity, as many other researchers have shown^{4-8, 10-14}. Thus, it is reasonable that Mel-CPS doped with N would be much more active than Mel-CPS without N (C-CPS).

Generally, graphitic, pyrrolic, and pyridinic N are widely recognized as active N species for N-doped carbon catalysts^{7, 34-37}. Of these three active N species, graphitic N has recently been proven to play a more vital role in improving catalysts' ORR performance by Bao et al.³³ and Knights et al.^{35, 38}.

However, something different was observed with our Mel-CPS and Fe-Mel-CPS catalysts. As discussed above, the ORR performance of Fe-Mel-CPS is much better than that of Mel-CPS. However, Fe-Mel-CPS has a much lower graphitic N content (0.17 at%, Fig. 5d) than Mel-CPS (0.54 at%, Fig. 5d) does. Conversely, the amounts of pyrrolic and pyridinic N in the two materials are almost the same. Obviously, the dissimilar ORR performance of these two catalysts cannot be explained simply by the differences in their graphitic N content or the total amounts of active N in each material.

It has previously been proven that the metallic impurities within doped carbon catalysts can dramatically influence the materials' electrocatalytic properties³⁶. Recently, Pumera and co-workers confirmed that the ORR activity of graphene could be improved by trace metal impurities^{39, 40}. Thus, we recognized that trace levels of Fe residue (e. g. Fe and Fe_3C) in Fe-Mel-CPS might be responsible for its high ORR activity.

To verify the role of Fe during the ORR process, we further removed Fe residue from the Fe-Mel-CPS material using a

second acid treatment with hydrochloric acid (for the preparation details, see ESI†). The Fe content of Fe-Mel-CPS before and after the second acid treatment was measured using ICP-AES.

The ICP-AES results suggest that the Fe content drops from 6.7 wt% to 2.2 wt% after the second acid treatment; in addition, the half-wave potential of its ORR curve decreases by 60 mV (Fig. 8), indicating the strong effect of Fe residue on the ORR performance of this doped carbon catalyst. In other words, the Fe residue may reasonably be another cause of the Fe-Mel-CPS catalyst's high electrocatalytic activity.

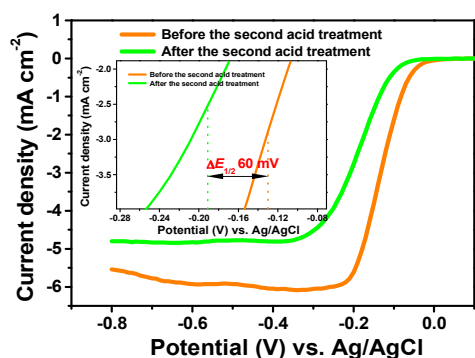


Fig. 8 ORR performances of Fe-Mel-CPS catalysts before and after the second acid treatment

From the results presented in Fig. 9, we can see that our Fe-Mel-CPS catalyst demonstrates excellent methanol tolerance and stability. As shown in Fig. 9a, the ORR performance at the Pt/C electrode displayed a significant drop in relative current density once methanol was introduced, while almost no apparent change was observed for the Fe-Mel-CPS electrode, suggesting that Fe-Mel-CPS has much better methanol tolerance than commercial Pt/C.

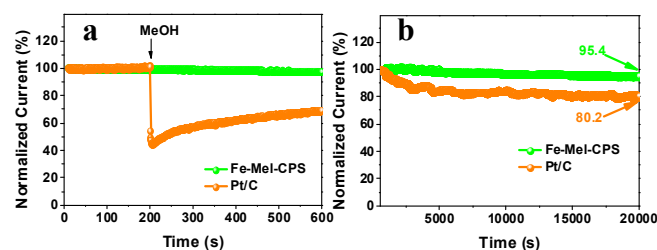


Fig. 9 (a) Current-time (*i-t*) chronoamperometric response of Fe-Mel-CPS and commercial 20% Pt/C electrodes when 3 M methanol is added after 200 s; (b) current-time (*i-t*) chronoamperometric response of Fe-Mel-CPS and commercial 20% Pt/C electrodes at -0.3 V in O_2 -saturated 0.1 M KOH at a rotation rate of 1600 rpm

Fig. 9b shows the excellent stability of Fe-Mel-CPS. After continuous O_2 reduction at -0.3 V (vs. Ag/AgCl) for 20 000 s, Fe-Mel-CPS electrode maintained more than 95% of its initial current density, whereas the Pt/C electrode lost almost 20% of its initial current density under the same conditions.

Conclusions

We successfully prepared a doped carbon catalyst with high surface area and hierarchical porous structures through a facile

non-template approach, in which cross-linked PS, melamine and ferric chloride were used as precursors. The catalyst exhibits excellent ORR performance, outstanding methanol tolerance, remarkable stability and nearly 100% selectivity for the four-electron ORR process. To our knowledge, it is also one of the most active ORR catalysts in alkaline media to date. Importantly, we find that residual Fe is as important as doped nitrogen for ORR performance enhancements. This catalyst's high ORR performance, outstanding stability and excellent methanol tolerance, combined with its hierarchical porous morphology, will make it promising for novel, environmentally friendly electrochemical energy systems, such as PEMFCs, DMFCs, and metal-air batteries. In addition, our work may also provide a way to turn polystyrene waste into wealth.

Acknowledgements

This work was supported by the National Natural Science Foundation of China (NSFC Project Nos. 21076089, 21276098, 11132004, U1301245), the Ministry of Science and Technology of China (Project No. 2012AA053402), the Guangdong Natural Science Foundation (Project No. S2012020011061), the Doctoral Fund of the Ministry of Education of China (20110172110012), and the Basic Scientific Foundation of the Central Universities of China (No. 2013ZP0013).

Notes and references

- ⁶⁰ *The Key Laboratory of Fuel Cell Technology of Guangdong Province, School of Chemistry and Chemical Engineering, South China University of Technology, Guangzhou, 510641, China, Fax: +86 20 8711 3586. E-mail address: chsjliao@scut.edu.cn*
- [†]Electronic Supplementary Information (ESI) available: more experimental details, additional SEM and TEM images, linear voltammetric curves, Koutecký–Levich plots, N_2 adsorption-desorption isotherms, and pore-size distributions. See DOI:
1. H. T. Chung, J. H. Won and P. Zelenay, *Nat Commun*, 2013, **4**, 1922-1926.
2. E. Proietti, F. Jaouen, M. Lefevre, N. Larouche, J. Tian, J. Herranz and J. P. Dodelet, *Nat Commun*, 2011, **2**, 416-424.
3. Y. Y. Liang, Y. G. Li, H. L. Wang, J. G. Zhou, J. Wang, T. Regier and H. J. Dai, *Nat Mater*, 2011, **10**, 780-786.
4. P. Zhang, F. Sun, Z. Xiang, Z. Shen, J. Yun and D. Cao, *Energ Environ Sci*, 2014, **7**, 442-450.
5. X. Zhong, H. Yu, G. Zhuang, Q. Li, X. Wang, Y. Zhu, L. Liu, X. Li, M. Dong and J.-g. Wang, *J Mater Chem A*, 2014, **2**, 897-901.
6. T. Palaniselvam, M. O. Valappil, R. Illathvalappil and S. Kurungot, *Energ Environ Sci*, 2013, **7**, 1059-1067.
7. G. Wu, K. L. More, C. M. Johnston and P. Zelenay, *Science*, 2011, **332**, 443-447.
8. J. B. Xu, P. Gao and T. S. Zhao, *Energ Environ Sci*, 2012, **5**, 5333-5339.
9. C. You, S. Liao, H. Li, S. Hou, H. Peng, X. Zeng, F. Liu, R. Zheng, Z. Fu and Y. Li, *Carbon*, 2014, **69**, 294-301.
10. H. L. Peng, Z. Y. Mo, S. J. Liao, H. G. Liang, L. J. Yang, F. Luo, H. Y. Song, Y. L. Zhong and B. Q. Zhang, *Sci Rep-Uk*, 2013, **3**.
11. Z. Mo, S. Liao, Y. Zheng and Z. Fu, *Carbon*, 2012, **50**, 2620-2627.
12. Y. Zheng, Y. Jiao, L. Ge, M. Jaroniec and S. Z. Qiao, *Angew Chem Int Edit*, 2013, **52**, 3110-3116.
13. J. Liang, Y. Zheng, J. Chen, J. Liu, D. Hulicova-Jurcakova, M. Jaroniec and S. Z. Qiao, *Angew Chem Int Edit*, 2012, **51**, 3892-3896.
14. Q. Shi, F. Peng, S. Liao, H. Wang, H. Yu, Z. Liu, B. Zhang and D. Su, *J Mater Chem A*, 2013, **1**, 14853-14857.
15. W. Kiciński, M. Szala and M. Bystrzejewski, *Carbon*, 2014, **68**, 1-32.

16. Y. G. Li, W. Zhou, H. L. Wang, L. M. Xie, Y. Y. Liang, F. Wei, J. C. Idrobo, S. J. Pennycook and H. J. Dai, *Nat Nanotechnol*, 2012, **7**, 394-400.
17. R. Bashyam and P. Zelenay, *Nature*, 2006, **443**, 63-66.
18. Z. Liu, H. G. Nie, Z. Yang, J. Zhang, Z. P. Jin, Y. Q. Lu, Z. B. Xiao and S. M. Huang, *Nanoscale*, 2013, **5**, 3283-3288.
19. J. Liang, X. Du, C. Gibson, X. W. Du and S. Z. Qiao, *Adv Mater*, 2013, **25**, 6226-6231.
20. J. Liang, Y. Jiao, M. Jaroniec and S. Z. Qiao, *Angew Chem Int Edit*, 2012, **51**, 11496-11500.
21. Y. Wang, X. Cui, Y. Li, L. Chen, H. Chen, L. Zhang and J. Shi, *Carbon*, 2014, **68**, 232-239.
22. Y. Zheng, Y. Jiao, J. Chen, J. Liu, J. Liang, A. Du, W. M. Zhang, Z. H. Zhu, S. C. Smith, M. Jaroniec, G. Q. Lu and S. Z. Qiao, *J Am Chem Soc*, 2011, **133**, 20116-20119.
23. F. Markoulidis, C. Lei, C. Lekakou, D. Duff, S. Khalil, B. Martorana and I. Cannavaro, *Carbon*, 2014, **68**, 58-66.
24. D. W. Wang, F. Li, M. Liu, G. Q. Lu and H. M. Cheng, *Angew Chem Int Edit*, 2008, **47**, 373-376.
25. S. Evers and L. F. Nazar, *Accounts Chem Res*, 2012, **46**, 1135-1143.
26. X. Ji, S. Evers, R. Black and L. F. Nazar, *Nat Commun*, 2011, **2**, 325-331.
27. M. Zhong, E. K. Kim, J. P. McGann, S. E. Chun, J. F. Whitacre, M. Jaroniec, K. Matyjaszewski and T. Kowalewski, *J Am Chem Soc*, 2012, **134**, 14846-14857.
28. Z. Tan, Z. H. Sun, H. H. Wang, Q. Guo and D. S. Su, *J Mater Chem A*, 2013, **1**, 9462-9468.
29. Z. Tan, Z. H. Sun, Q. Guo, H. H. Wang and D. S. Su, *J Mater Sci Technol*, 2013, **29**, 609-612.
30. Z. H. Sun, L. F. Wang, P. P. Liu, S. C. Wang, B. Sun, D. Z. Jiang and F. S. Xiao, *Adv Mater*, 2006, **18**, 1968-1971.
31. C. Zou, D. C. Wu, M. Z. Li, Q. C. Zeng, F. Xu, Z. Y. Huang and R. W. Fu, *J Mater Chem*, 2010, **20**, 731-735.
32. L. Sun, C. Tian, M. Li, X. Meng, L. Wang, R. Wang, J. Yin and H. Fu, *J Mater Chem A*, 2013, **1**, 6462-6470.
33. J. Wang, G. Wang, S. Miao, X. Jiang, J. Li and X. Bao, *Carbon*, 2014, **75**, 381-389.
34. D. Wang and D. S. Su, *Energ Environ Sci*, 2014, **7**, 576-591.
35. L. F. Lai, J. R. Potts, D. Zhan, L. Wang, C. K. Poh, C. H. Tang, H. Gong, Z. X. Shen, L. Y. Jianyi and R. S. Ruoff, *Energ Environ Sci*, 2012, **5**, 7936-7942.
36. D. H. Deng, X. L. Pan, L. A. Yu, Y. Cui, Y. P. Jiang, J. Qi, W. X. Li, Q. A. Fu, X. C. Ma, Q. K. Xue, G. Q. Sun and X. H. Bao, *Chem Mater*, 2011, **23**, 1188-1193.
37. G. Liu, X. G. Li, P. Ganesan and B. N. Popov, *Electrochim Acta*, 2010, **55**, 2853-2858.
38. D. S. Geng, Y. Chen, Y. G. Chen, Y. L. Li, R. Y. Li, X. L. Sun, S. Y. Ye and S. Knights, *Energ Environ Sci*, 2011, **4**, 760-764.
39. L. Wang, A. Ambrosi and M. Pumera, *Angew Chem Int Edit*, 2013, **52**, 13818-13821.
40. C. H. A. Wong, C. K. Chua, B. Khezri, R. D. Webster and M. Pumera, *Angew Chem Int Edit*, 2013, **125**, 8847-8850.

55

Graphical Abstract

High performance carbon-based ORR catalyst with ultra-high surface area and hierarchical porous structures derived from polystyrene foam waste.

